J. Fluid Mech. (2014), *vol.* 744, *pp.* 89–110. © Cambridge University Press 2014
doi:10.1017/jfm.2014.84

Spin-up of a two-component superfluid: self-consistent container feedback

Cornelis A. van Eysden† and A. Melatos

School of Physics, University of Melbourne, Parkville, VIC 3010, Australia

(Received 16 September 2013; revised 23 December 2013; accepted 6 February 2014; first published online 10 March 2014)

The coupled dynamic response of a rigid container filled with a two-component superfluid undergoing Ekman pumping is calculated self-consistently. The container responds to the back-reaction torque exerted by the viscous component of the superfluid and an arbitrary external torque. The resulting motion is described by a pair of coupled integral equations for which solutions are easily obtained numerically. If the container is initially accelerated impulsively then set free, it relaxes quasi-exponentially to a steady state over multiple time scales, which are a complex combination of the Ekman number, superfluid mutual friction coefficients, the superfluid density fraction, and the varying hydrodynamic torque at different latitudes. The spin-down of containers with relatively small moments of inertia (compared with that of the contained fluid) depends weakly on the above parameters and occurs faster than the Ekman time. When the fluid components are initially differentially rotating, the container can 'overshoot' its asymptotic value before increasing again. When a constant external torque is applied, the superfluid components rotate differentially and non-uniformly in the long term. For an oscillating external torque, the amplitude and phase of the oscillation are most sensitive to the driving frequency for containers with relatively small moments of inertia. Applications to superfluid helium experiments and neutron stars are also discussed.

Key words: geophysical and geological flows, quasi-geostrophic flows, rotating flows

1. Introduction

The spin-up of a rotating fluid in response to an impulsive acceleration of its container has been studied extensively (Benton & Clark 1974; Duck & Foster 2001). Since Greenspan & Howard (1963) calculated the linear spin-up of an incompressible Navier–Stokes fluid, the theory of spin-up has been generalized in numerous directions, including stratified flows (Pedlosky 1967; Walin 1969; Clark *et al.* 1971; Hewitt *et al.* 1999), compressible fluids (Abney & Epstein 1996; van Eysden & Melatos 2008; Bennett, van Eysden & Melatos 2010) and electrically conducting or hydromagnetic flows (Benton & Loper 1969; Loper 1971; Easson 1979; Abney, Epstein & Olinto 1996; Mendell 1998). The spin-up of multi-component fluids has also been studied to model superfluids such as helium II (Reisenegger 1993) as well as the separation of fluid–particle mixtures in batch centrifuges (Amberg & Ungarish 1993). The above

† Email address for correspondence: ave@unimelb.edu.au

https://doi.org/10.1017/jfm.2014.84 Published online by Cambridge University Press

studies are restricted to situations where the rotation of the container is completely prescribed before and after its impulsive acceleration. The coupled spin-up of a fluid and its container has not been studied numerically or analytically in the literature.

In a previous paper (van Eysden & Melatos 2013), we presented the first analytic solution for the spin-up of a Hall–Vinen–Bekharevich–Khalatnikov (HVBK) superfluid in arbitrary geometry, in response to a container whose rotation is prescribed. In the present paper, we generalize this calculation to describe a container that responds to the torque exerted by the fluid within. An external non-hydrodynamic driving torque is also included for completeness.

Two primary motivations exist for this study. First, a self-consistent theory of the coupled spin-up of a two-component superfluid and its container is an essential ingredient for understanding a long-standing question in astrophysics: the phenomenon of pulsar glitches (Lyne, Shemar & Smith 2000; Wang *et al.* 2000; Melatos, Peralta & Wyithe 2008; Espinoza *et al.* 2011). Glitches are tiny, impulsive, randomly timed increases in the spin frequency of a rotation-powered pulsar, during which angular momentum stored in the superfluid interior of the neutron star is transferred erratically to the solid crust (Anderson & Itoh 1975; Warszawski & Melatos 2011). Following a glitch, the crust experiences a quasi-exponential recovery phase, during which it responds to the torque exerted by the internal fluid (Reisenegger & Goldreich 1992; Peralta *et al.* 2005), and superfluidity is expected to play a key role (Lyne & Graham-Smith 1998). The theory of coupled spin-up developed in this article can be combined with radio-telescope observations of glitch recovery to measure the transport coefficients of bulk nuclear matter at densities $\gtrsim 10^{15}$ g cm^{-3}, the only way at present that such measurements can be made (van Eysden & Melatos 2010).

Second, a theory of coupled superfluid–container spin-up is necessary to interpret laboratory experiments involving the spin-up of helium II. A comprehensive collection of such experiments was performed by the Tsakadze group over a decade, to measure the response of superfluid-filled containers following an impulsive increase in angular velocity (Tsakadze & Tsakadze 1972, 1973, 1974, 1980). Reisenegger (1993) sought to explain the data by solving the spin-up problem between slowly accelerating parallel plates, but the analysis does not treat the coupled motion of the fluid and container self-consistently, and considers the wrong geometry. In contrast, the theory presented in this paper can be directly compared with the experimentally observed container response.

Many other applications exist for the general theory presented here. For example, a pulsar crust spins down in response to an electromagnetic dipole torque arising from a magnetic field (which is frozen into its crust) as well as the hydrodynamic torque arising from Ekman pumping in the stellar interior (Lyne & Graham-Smith 1998). Alternatively, the dynamic response of superfluid-filled containers, like that measured by Tsakadze & Tsakadze (1980), can be fitted to the theory, allowing unknown mutual friction and viscosity coefficients to be extracted. These applications are discussed in companion papers (van Eysden & Melatos 2012, 2011).

This paper is structured as follows. In § 2 a summary of the model assumptions and relevant results from the companion paper (van Eysden & Melatos 2013) is presented. In § 3, we solve for the motion of the container using the results derived in van Eysden & Melatos (2013) and torque balance on the container. The free response of the container and the interior fluid are investigated in § 4, for containers of varying geometries and moments of inertia. In § 5, the motion of the container in response to both a constant and oscillatory driving torque is investigated. The conclusions are presented in § 6.

https://doi.org/10.1017/jfm.2014.84 Published online by Cambridge University Press

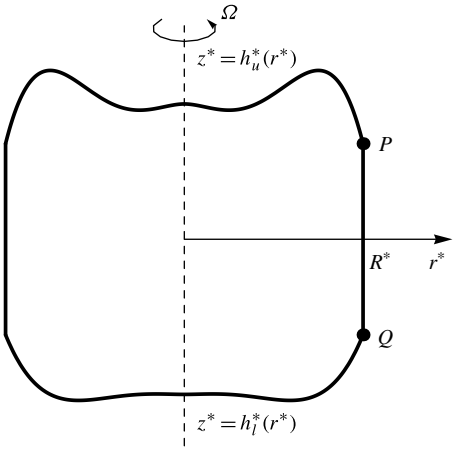


FIGURE 1. Schematic diagram of an axisymmetric container with upper (u) and lower (l) boundaries $z^* = h_{u,l}^*(r^*)$, rotating about the vertical axis $r^* = 0$. The analysis in this paper is equally valid whether or not P and Q coincide or are joined by a vertical boundary.

2. Superfluid equations of motion

Consider a simply connected container of the form drawn in figure 1 filled with a two-component superfluid, comprising an irrotational 'superfluid' component (i.e. a condensate) denoted with subscript s, and a dissipative 'normal' component with subscript n, e.g. helium II. The upper (u) and lower (l) surfaces of the container are described by the functions $z^* = h_{u,l}^*(r^*)$, where (r^*, ϕ, z^*) denote the usual cylindrical coordinates. The container is symmetric about the z^* axis. Its upper ($z^* \geqslant 0$) and lower ($z^* \leqslant 0$) halves can rotate separately in general; they slide freely along a contact curve $z^* = 0$, $r^* = R^*$, with R^* defined as the equatorial radius of the container where the sidewall joining the upper and lower surfaces intersects the midplane $z^* = 0$ (as in figure 1, where $h_{u,l}^*(R^*) \neq 0$) or where the upper and lower surfaces meet the midplane ($h_{u,l}^*(R^*) = 0$, as in a sphere).

Suppose the container rotates initially about the z^* axis with angular velocity Ω such that the Ekman number

$$E = \frac{\nu_n}{L^2\Omega} \ll 1, \tag{2.1}$$

is small. In (2.1), ν_n is the kinematic viscosity of the viscous component of the superfluid (the shear viscosity divided by the viscous component density fraction (Vinen & Niemela 2002)), and L is a fiducial length scale for the container. At $t = 0$, the container is impulsively accelerated, and the interior superfluid spins up via Ekman pumping over the characteristic time $E^{-1/2}\Omega^{-1}$. The transient and steady-state response of the fluid was calculated in van Eysden & Melatos (2013), by solving the two-fluid HVBK equations of motion for boundary conditions that evolve arbitrarily with time. The HVBK equations describe a two-component superfluid, coupled by the mutual friction force

$$\boldsymbol{F} = \tfrac{1}{2}B\hat{\boldsymbol{\omega}}_s^* \times [\boldsymbol{\omega}_s^* \times (\boldsymbol{v}_n^* - \boldsymbol{v}_s^*)] + \tfrac{1}{2}B'\boldsymbol{\omega}_s^* \times (\boldsymbol{v}_n^* - \boldsymbol{v}_s^*), \tag{2.2}$$

where $\boldsymbol{v}_{n,s}^*$ are the velocities of the 'normal' (i.e. viscous, subscript n) and 'superfluid' (i.e. inviscid, subscript s) components, $\boldsymbol{\omega}_s^* = \nabla \times \boldsymbol{v}_s^*$ is the macroscopic vorticity of

https://doi.org/10.1017/jfm.2014.84 Published online by Cambridge University Press

the inviscid component, and B and B' are the mutual friction coefficients. The total velocity is defined as

$$\boldsymbol{v}^* = \rho_n \boldsymbol{v}_n^* + \rho_s \boldsymbol{v}_s^*, \tag{2.3}$$

where $\rho_{n,s}$ are the viscous and inviscid component density fractions.

The spin-up flow of a two-component fluid depends strongly on the relative size of B and E. When the mutual friction is strong ($B \sim 1$), the azimuthal inviscid and viscous components lock together, i.e. differential rotation is removed over the rotational time scale Ω^{-1}. Ekman pumping occurs in the inviscid component, because it is dragged along by the viscous component via the mutual friction. For intermediate coupling ($B \sim E^{1/2}$), the azimuthal components come into co-rotation over the time scale $B^{-1}\Omega^{-1}$; there is no Ekman pumping in the inviscid component, because the mutual friction is too weak. For weak coupling ($B \ll E^{1/2}$), the viscous component spins up virtually uninhibited by the inviscid component, which spins up over the much longer mutual friction time scale $B^{-1}\Omega^{-1}$.

The impulsive angular acceleration occurs as follows. For $t \leqslant 0$, the viscous and inviscid components rotate rigidly but differentially, with $\boldsymbol{v}_n^* = r^*\Omega_{n0}^*$ and $\boldsymbol{v}_s^* = r^*\Omega_{s0}^*$ in the rotating frame. The upper and lower boundaries also rotate differentially, with $\boldsymbol{v}_u^* = r^*\epsilon\Omega f_u(t)\boldsymbol{e}_\phi$ and $\boldsymbol{v}_l^* = r^*\epsilon\Omega f_l(t)\boldsymbol{e}_\phi$, respectively, where $\epsilon \ll 1$ is the Rossby number. In van Eysden & Melatos (2013), $f_u(t)$ and $f_l(t)$ are prescribed; the aim of the present paper is to determine $f_u(t)$ and $f_l(t)$ self-consistently when the container responds to the hydrodynamic torque.

The walls of the container are assumed to be smooth, so that pinning is neglected. Consequently, the vortex tension only plays a passive role in the boundary layer and can be neglected, as discussed in detail in § 2.2 of van Eysden & Melatos (2013). Under these assumptions, the required boundary conditions are no-slip for the viscous component, while no-penetration suffices for the inviscid component. In general, a superfluid has a hysteretic response to external rotation because of the superfluidity (Jones *et al.* 1995; Jackson & Barenghi 2006). In smooth-walled containers, the critical velocity for vortex nucleation at the wall is larger than in the bulk, which can result in the formation of a vortex-free region near the wall. If there is roughness or vortex pinning on the container wall (e.g. in the crust of a neutron star), the hysteric effect can be suppressed, because the nucleation critical velocity (or vortex stretching due to pinning) increases at a smoother wall (Parker & Adams 2006; Goldbaum & Mueller 2009; Warszawski, Melatos & Berloff 2012). This hysteretic effect is neglected in this paper, and it is assumed that both the viscous and inviscid components rotate uniformly for $t \leqslant 0$ according to the initial conditions above.

The vortex tension plays an important role in superfluid turbulence, which may arise from, for example, the Glaberson–Donnelly instability (Glaberson, Johnson & Ostermeier 1974; Donnelly 2005). This and other instabilities are discussed in detail in § 2.2 of the companion paper (van Eysden & Melatos 2013) and the application papers (van Eysden & Melatos 2010, 2011, 2012), where it is shown that turbulence does not play a role in the parameter range considered.

2.1. *Viscous torque*

The viscous torque exerted on the container by the interior flow was calculated in § 5 of van Eysden & Melatos (2013). The result is expressed in terms of scaled variables, $t^* = E^{-1/2}\Omega^{-1}\tau$, $r^* = Lr$, $z^* = Lz$, $h^*(r^*) = Lh(r)$, $\boldsymbol{v}_{n,s}^* = \epsilon\Omega L\boldsymbol{v}_{n,s}$ and $T_{u,l}^{*h} = \rho L^5\epsilon\Omega^2 T_{u,l}^h$,

https://doi.org/10.1017/jfm.2014.84 Published online by Cambridge University Press

where an asterisk is used to distinguish a dimensional variable from its dimensionless counterpart. The viscous torque on the upper and lower surfaces is

$$T_u^h = -2\pi E^{1/2} \int_0^R \mathrm{d}r \left(\frac{J_u r^2}{J_u + J_l}\right) \left[(h_u + h_l)\frac{\partial v_\phi^I}{\partial \tau} + rJ_l(f_u - f_l)\right], \tag{2.4}$$

$$T_l^h = -2\pi E^{1/2} \int_0^R \mathrm{d}r \left(\frac{J_l r^2}{J_u + J_l}\right) \left[(h_u + h_l)\frac{\partial v_\phi^I}{\partial \tau} - rJ_u(f_u - f_l)\right], \tag{2.5}$$

where $v_\phi^I(r,\ \tau)$ is the leading-order (in $E^{1/2}$) total azimuthal velocity, which is columnar (independent of z) according to the Taylor–Proudman theorem. In (2.4) and (2.5) we define

$$J_{u,l} = \frac{\rho_n H_{u,l}^2}{2\lambda_{u,l-}(1 + H_{u,l}^4)}[|\lambda_{u,l}|^2(1 - H_{u,l}^4) + 4\lambda_{u,l-}^2 H_{u,l}^4], \tag{2.6}$$

with

$$\lambda_{u,l\pm} = \frac{1}{H_{u,l}} \left\{ \left[\frac{(B' - 2)^2 + B^2}{(\rho_n B' - 2)^2 + (\rho_n B)^2}\right]^{1/2} \mp \frac{\rho_s B(1 + H_{u,l}^4)}{H_{u,l}^2[(\rho_n B' - 2)^2 + (\rho_n B)^2]} \right\}^{1/2}, \tag{2.7}$$

$$H_{u,l}(r) = \left\{1 + \left[\frac{\mathrm{d}h_{u,l}(r)}{\mathrm{d}r}\right]^2\right\}^{1/4}, \tag{2.8}$$

$$|\lambda_{u,l}|^2 = \lambda_{u,l-}^2 + \lambda_{u,l+}^2. \tag{2.9}$$

For configurations with $h_{u,l}^*(R^*)$ (e.g. a cylinder), two nested boundary layers of thickness $E^{1/4}L$ and $E^{1/3}L$, known as Stewartson layers, form at the vertical walls (e.g. PQ in figure 1). The torques generated in these boundary layers scale as $O(E^{1/4})$ and $O(E^{1/3})$; however, we neglect them here for the sake of simplicity. The detailed structure of the Stewartson layers is discussed in the literature (Stewartson 1953; Pedlosky 1967; Greenspan 1968). For configurations with $h_{u,l}^*(R^*) = 0$ (e.g. spheres and cones), a singularity occurs in v_ϕ^I at $r^* = R^*$ and $z^* = 0$, which arises from the assumption that the derivatives with respect to $\zeta_{u,l}$ dominate those with respect to $\xi_{u,l}$ in the boundary layers; see Glampedakis & Andersson (2006) for a more detailed discussion. The singularity does not pose a problem in the present analysis because, upon performing the integrals in (2.4) and (2.5), the total torque is finite.

3. Container motion

3.1. *General solution*

In general, the rigid container experiences a viscous torque exerted by the viscous component of the superfluid plus an external driving torque supplied by, for example, a driving motor or friction in the apparatus. Torque balance on the upper/lower half of the container yields

$$I_{u,l}^* \frac{\mathrm{d}(\epsilon \Omega f_{u,l})}{\mathrm{d}t} = T_{u,l}^{*h} + T_{u,l}^{*ext}, \tag{3.1}$$

where the superscripts h and ext denote the viscous and external torques, respectively. Inserting (2.4) and (2.5) into (3.1), integrating subject to the initial conditions $v_\phi^I = r\Omega_0$, $f_u = f_{u0}$ and $f_l = f_{l0}$ at $\tau = 0$ (in the rotating frame), and writing the result in

https://doi.org/10.1017/jfm.2014.84 Published online by Cambridge University Press

dimensionless form, we obtain

$$f_u(\tau) = -\frac{2\pi K_u}{I_f}\int_0^R \mathrm{d}r\left(\frac{J_u r^2}{J_u+J_l}\right)\left[(h_u+h_l)(v_\phi^I - r\Omega_0) + rJ_l\int_0^\tau \mathrm{d}\tau'\,(f_u - f_l)\right] + f_{u0} + \frac{K_u}{I_f E^{1/2}}\int_0^\tau \mathrm{d}\tau'\,T_u^{ext}, \tag{3.2}$$

$$f_l(\tau) = -\frac{2\pi K_l}{I_f}\int_0^R \mathrm{d}r\left(\frac{J_l r^2}{J_u+J_l}\right)\left[(h_u+h_l)(v_\phi^I - r\Omega_0) - rJ_u\int_0^\tau \mathrm{d}\tau'\,(f_u - f_l)\right] + f_{l0} + \frac{K_l}{I_f E^{1/2}}\int_0^\tau \mathrm{d}\tau'\,T_l^{ext}. \tag{3.3}$$

In (3.2) and (3.3), we define $K_{u,l} = I_f^*/I_{u,l}^*$ as the ratio of the moment of inertia of the total contained fluid (rotating notionally as a rigid body) to the moment of inertia of the upper/lower half of the container. We also write

$$I_f = \frac{I_f^*}{\rho L^5} = 2\pi\int_0^R \mathrm{d}r\, r^3(h_u+h_l), \tag{3.4}$$

where $\mathrm{d}V = 2\pi r(h_u+h_l)\mathrm{d}r$ is the volume of a fluid column of height (h_u+h_l). The quantities $h_{u,l}$, $J_{u,l}$ and Ω_0 are functions of r only, $f_{u,l}$ and $T_{u,l}^{ext}$ depend on τ only, and v_ϕ depends on r and τ.

To solve for the motion of the container, we substitute the result for $v_\phi^I(r,\tau)$, given by (2.83) in van Eysden & Melatos (2013) into (3.2) and (3.3). Assuming Ω_0 and Ω_{n0} are constant (i.e. both fluid components are rotating uniformly at $\tau = 0$), the results can be written as

$$\begin{aligned} f_u(\tau) = {} & -K_u\int_0^\tau \mathrm{d}\tau'\{[\dot g_{uu}^A(\tau-\tau') + \dot g_{uu}^B(\tau-\tau')]f_u(\tau') \\ & + [\dot g_{ul}^A(\tau-\tau') + \dot g_{ul}^B(\tau-\tau')]f_l(\tau')\} \\ & + K_u\{[g_{uu}^A(\tau) + g_{ul}^A(\tau)]\Omega_{n0} + [g_{uu}^B(\tau) + g_{ul}^B(\tau)]\Omega_0\} \\ & - K_u\dot g_{ul}^A(0)\int_0^\tau \mathrm{d}\tau'\,[f_u(\tau') - f_l(\tau')] + f_{u0} + \frac{K_u}{I_f E^{1/2}}\int_0^\tau \mathrm{d}\tau'\,T_u^{ext}, \end{aligned} \tag{3.5}$$

$$\begin{aligned} f_l(\tau) = {} & -K_l\int_0^\tau \mathrm{d}\tau'\{[\dot g_{ul}^A(\tau-\tau') + \dot g_{ul}^B(\tau-\tau')]f_u(\tau') \\ & + [\dot g_{ll}^A(\tau-\tau') + \dot g_{ll}^B(\tau-\tau')]f_l(\tau')\} \\ & + K_l\{[g_{ul}^A(\tau) + g_{ll}^A(\tau)]\Omega_{n0} + [g_{ul}^B(\tau) + g_{ll}^B(\tau)]\Omega_0\} \\ & + K_l\dot g_{ul}^A(0)\int_0^\tau \mathrm{d}\tau'\,[f_u(\tau') - f_l(\tau')] + f_{l0} + \frac{K_l}{I_f E^{1/2}}\int_0^\tau \mathrm{d}\tau'\,T_l^{ext}. \end{aligned} \tag{3.6}$$

In (3.5) and (3.6) we define

$$g_{xy}^A(\tau) = -\frac{2\pi}{I_f}\int_0^R \mathrm{d}r\, r^3\frac{J_xJ_y(\mathrm{e}^{\omega_+\tau} - \mathrm{e}^{\omega_-\tau})}{(J_u+J_l)(\omega_- - \omega_+)}, \tag{3.7}$$

$$\begin{aligned} g_{xy}^B(\tau) &= \beta\int_0^\tau \mathrm{d}\tau' g_{xy}^A(\tau'), \\ &= -\frac{2\pi}{I_f}\int_0^{r_o} \mathrm{d}r\, r^3\frac{J_xJ_y(h_u+h_l)[\omega_-(\mathrm{e}^{\omega_+\tau}-1) - \omega_+(\mathrm{e}^{\omega_-\tau}-1)]}{(J_u+J_l)^2(\omega_- - \omega_+)}, \end{aligned} \tag{3.8}$$

https://doi.org/10.1017/jfm.2014.84 Published online by Cambridge University Press

where x, y refer to either u or l, an overdot denotes a derivative with respect to τ, and we have

$$\omega_{\pm} = -\frac{1}{2}\left(\beta + \frac{I_u + I_l}{h_u + h_l}\right) \pm \left\{\left[\frac{1}{2}\left(\beta + \frac{I_u + I_l}{h_u + h_l}\right)\right]^2 - \beta\left(\frac{J_u + J_l}{h_u + h_l}\right)\right\}^{1/2}, \tag{3.9}$$

$$I_{u,l} = \frac{1}{|\lambda_{u,l}|^2 \lambda_{u,l-}}\left[\left(\frac{1 - H_{u,l}^4}{1 + H_{u,l}^4}\right)^2 \left(\lambda_{u,l+}^2 - \lambda_{u,l-}^2\right)^2 + 4\lambda_{u,l+}^2 \lambda_{u,l-}^2\right]^{1/2}, \tag{3.10}$$

$$\beta = \frac{2BE^{-1/2}}{2 - B'}. \tag{3.11}$$

The functions (3.7) and (3.8) can be evaluated for arbitrary geometry, Ekman number E, mutual friction coupling constants B, B', and viscous component density fraction ρ_n. Therefore, (3.5) and (3.6) are a coupled pair of integral equations for the unknowns $f_u(\tau)$ and $f_l(\tau)$. The system cannot be solved analytically. Numerically, one proceeds by guessing trial functions (e.g. exponentials) for f_u and f_l and iterating until convergence is obtained. This can be done efficiently in any symbolic algebra package, e.g. Mathematica or Matlab; we do it in §§ 4 and 5 for some interesting cases. Once $f_u(\tau)$ and $f_l(\tau)$ are determined, the interior azimuthal flow can be computed from (2.83) and (2.84) with boundary layer corrections (2.66)–(2.70) in van Eysden & Melatos (2013). The streamfunction for the poloidal flow is computed from (2.85) and (2.86) with boundary layer corrections (2.58)–(2.65) in van Eysden & Melatos (2013).

3.2. *Angular momentum conservation*

Equations (3.2) and (3.3) imply conservation of angular momentum. Evaluating $f_u/K_u + f_l/K_l$, and restoring dimensional variables, we find

$$\begin{aligned}&\epsilon\Omega[I_u^* f_{u0} + I_l^* f_{l0}] + 2\pi\rho\int_0^{R*} \mathrm{d}r^*\, r^{*3}(h_u^* + h_l^*)\Omega_0^* + \int_0^t \mathrm{d}t'\,(T_u^{*ext} + T_l^{*ext}) \\ &\quad = \epsilon\Omega[I_u^* f_u(t) + I_l^* f_l(t)] + 2\pi\rho\int_0^{R^*} \mathrm{d}r^*\, r^{*2}(h_u^* + h_l^*)v_\phi^{*I}.\end{aligned} \tag{3.12}$$

On the left-hand side, in order from left to right, the terms correspond to the initial angular momentum of the upper and lower container lids and the fluid, respectively (where a column of fluid of height $h_u^* + h_l^*$ at radius r^* has velocity $r^*\Omega_0^*$) and the angular impulse imparted to the system by the external torque by time t. This equals, on the right-hand side, the angular momentum of the upper and lower container lids and the fluid at time t. Therefore, angular momentum is conserved.

3.3. *One-piece containers*

In many practical applications, the upper and lower surfaces are rigidly locked together. Then (3.5) and (3.6) reduce to a single equation. Writing $f_u(\tau) = f_l(\tau) = f(\tau)$, we find that a torque balance leads to

$$\begin{aligned}f(\tau) \;=\; &-K\int_0^\tau \mathrm{d}\tau'\,[\dot{g}^A(\tau - \tau') + \dot{g}^B(\tau - \tau')]f(\tau') \\ &+ Kg^A(\tau)\Omega_{n0} + Kg^B(\tau)\Omega_0 + f_0 + \frac{K}{I_f E^{1/2}}\int_0^\tau \mathrm{d}\tau' T^{ext}(\tau'),\end{aligned} \tag{3.13}$$

https://doi.org/10.1017/jfm.2014.84 Published online by Cambridge University Press

where $K = (K_u^{-1} + K_l^{-1})^{-1}$ is the ratio of the moment of inertia of the fluid (rotating nominally as a rigid body) to the moment of inertia of the entire container, and T^{ext} is the total external torque on the container. Equations (3.7) and (3.8) reduce to

$$\begin{aligned} g^A(\tau) &= g^A_{uu}(\tau) + 2g^A_{ul}(\tau) + g^A_{ll}(\tau) \\ &= -\frac{2\pi}{I_f}\int_0^R \mathrm{d}r\, r^3 \left(\frac{J_u + J_l}{\omega_- - \omega_+}\right)(\mathrm{e}^{\omega_+\tau} - \mathrm{e}^{\omega_-\tau}), \end{aligned} \tag{3.14}$$

$$\begin{aligned} g^B(\tau) &= \beta \int_0^\tau g^A(\tau')\mathrm{d}\tau' \\ &= 1 - \frac{2\pi}{I_f}\int_0^R \mathrm{d}r\, \frac{r^3(h_u + h_l)(\omega_-\mathrm{e}^{\omega_+\tau} - \omega_+\mathrm{e}^{\omega_-\tau})}{\omega_- - \omega_+}. \end{aligned} \tag{3.15}$$

In a cylinder, where one has $h_u(r) = h_l(r) = 1$, equations (2.6)–(2.9), (3.9) and (3.10) are independent of r, and an analytic solution can be obtained. The result is presented in the following section (see (5.8)). Other special cases of interest, including that of a single-component Navier–Stokes fluid, are presented in appendix A.

4. Free response

The solutions to (3.5) and (3.6) enjoy many practical applications, which will be explored in future papers. In this section and the next, we explore the physics arising from the interaction between the fluid and the container. First, we consider the free response, i.e. the case with no external torque.

4.1. *Effect of changing K*

We begin by investigating the effect of changing the moment of inertia of the container, parametrized by $K_{u,l}$; the superfluid parameters B, B', E and ρ_n have been explored in van Eysden & Melatos (2013). For simplicity, we consider the spin-down of a one-piece cylindrical container, where the results from § 3.3 apply. In figure 2, we present the response of the container to an impulsive acceleration. This can be modelled in (3.13) in two equivalent ways: taking $f_0 = 1$ at $\tau = 0$ with $T^{ext}(\tau) = 0$; or $f_0 = 0$ and $T^{ext}(\tau) = \delta(\tau)$. For all curves, the superfluid components are initially co-rotating with each other, i.e. $\Omega_0 = \Omega_{n0} = 0$. We choose $B' = 0$, $\rho_n = 0.5$ and $E = 0.005$.

Three values of K are presented: $K = 0.1$ (top curves), $K = 1$ (centre curves) and $K = 10$ (bottom curves), corresponding to a large, equal and small moment of inertia of the container (relative to that of the fluid rotating as a rigid body), respectively. In the experiments of Tsakadze & Tsakadze (1980) we have $K = 0.8$ (van Eysden & Melatos 2011), while in a neutron star it is predicted that $K \sim 50$ (van Eysden & Melatos 2010). The solid curves represent strong coupling ($B = 1$), and dashed curves represent intermediate coupling ($B = 0.071$). For each value of K, the responses for the strong and intermediate coupling approach the same steady state, as required by angular momentum conservation. The spin-down time of the container t_0 is defined as the time at which the difference between the angular velocity of the container and its steady-state angular velocity drops to 27 % (e^{-1}) of its original value. t_0 is longer for larger K, where the container has a greater moment of inertia. Time t_0 is also longer when the mutual friction is weaker, because the inviscid component takes longer to respond.

https://doi.org/10.1017/jfm.2014.84 Published online by Cambridge University Press

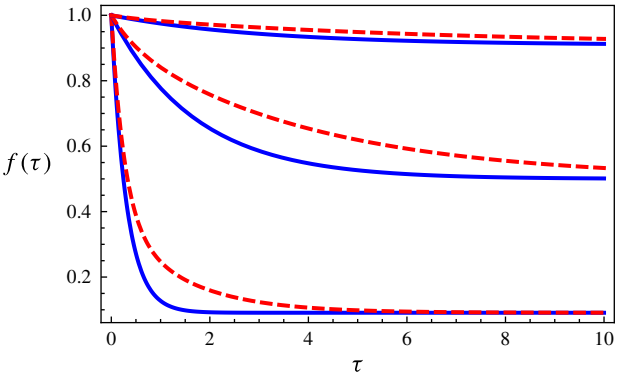


FIGURE 2. (Colour online) Spin-down of a spherical container following an impulsive acceleration. The top pair of curves corresponds to $K = 0.1$; centre curves $K = 1$; bottom curves $K = 10$. Solid lines (blue online) represent strong coupling, with $B = 1$; dashed lines (red online) represent intermediate coupling, with $B = 0.071$. The other parameters are $\Omega_0 = \Omega_{n0} = 0$ and we take $B' = 0$, $\rho_n = 0.25$ and $E = 0.005$.

In figure 3, we plot contours for t_0 in a cylinder as a function of B and E, for (*a*) $K = 1$ and (*b*) $K = 10$. The parameters B and E are chosen as they have the strongest impact; see van Eysden & Melatos (2013). For simplicity we only consider $\Omega_{n0} = \Omega_0 = 0$, to avoid non-monotonic spin-down (see § 4.2). Comparing figure 3(*a*) and (*b*), we see that t_0 depends weakly on B and E when K is large (panel (*b*)), corresponding to a light container that spins down almost immediately. When the inertia of the container is comparable to that of the fluid (panel (*a*)), t_0 depends more strongly on B and E. For large B, the fluids are strongly coupled by mutual friction and t_0 is approximately the Ekman time. For small B, t_0 is much longer because the inviscid component of the fluid takes longer to spin up. These trends carry over to other geometries, as the shape of the container primarily affects the shape of the spin-down curve, rather than t_0 (see § 4.2).

4.2. *Geometry*

In figure 4, we graph the angular velocity of the container versus time for three different geometries. The solid, dashed and dot-dashed curves correspond to a cylinder, sphere and cone, respectively, with $K = 1$, $B = 1$, $B' = 0$, $E = 0.005$, $\rho_n = 0.25$ and $\Omega_0 = \Omega_{n0} = 0$. The solution in cylindrical geometry is exact and given by (5.8)–(5.12) (see below) with $A = 0$. In all cases we choose $R = 1$ to ensure a fair comparison, i.e. the radius of the sphere equals the radius and half-height of the cylinder and the base radius and half-height of the cone.

The three geometries have different spin-down curves. This arises because the torque exerted on the container by the fluid varies with geometry. In a sphere and a cone, the torque exerted by a column of fluid between r and $r + \mathrm{d}r$ varies with r, while in a cylinder it does not. Where the container is shorter, the spin-up time for the fluid is faster, and the torque exerted on the container is larger. The torque on spheres and cones is a weighted sum of the varying torques at different r, resulting in a quasi-exponential container spin-down. In a cylinder the torque is uniform, resulting in exponential spin-down. The spin-down of a container is only exponential in cylindrical geometry; in all other geometries, it is quasi-exponential, even for a one-component Navier–Stokes fluid.

https://doi.org/10.1017/jfm.2014.84 Published online by Cambridge University Press

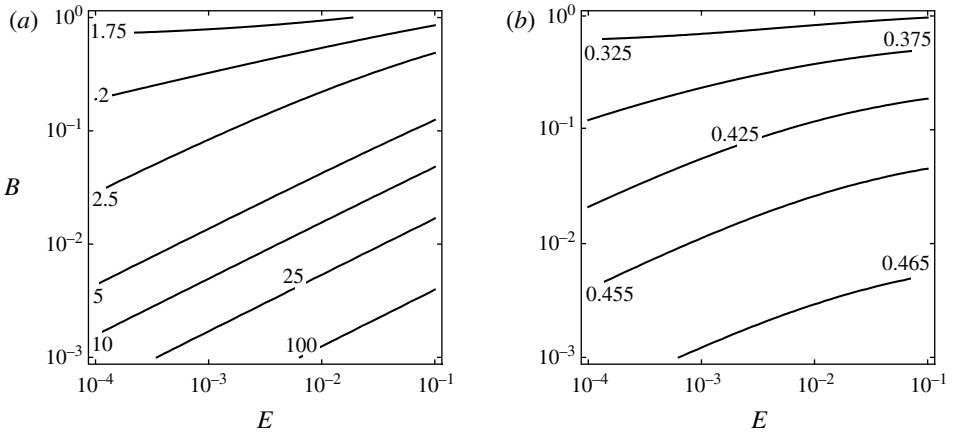


FIGURE 3. Contour plots for the spin-down time of a cylinder following an impulsive increase in angular velocity as a function of B and E: (*a*) $K = 1$ with contours 1.75, 2.0, 2.5, 5.0, 10, 25, 100; (*b*) $K = 10$ with contours 0.325, 0.375, 0.425, 0.455, 0.465. In both panels $\rho_n = 0.25$, $B' = 0$ and $\Omega_{n0} = \Omega_0 = 0$.

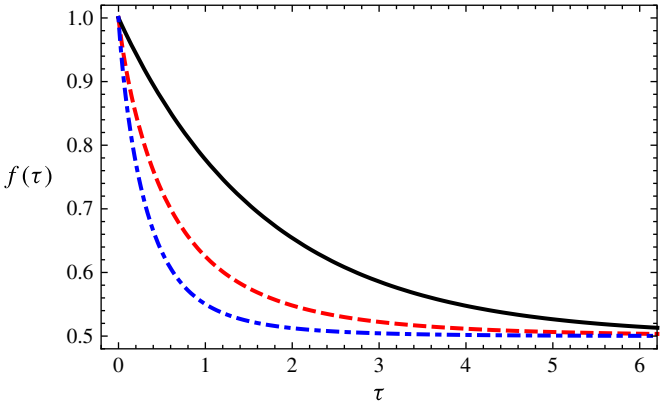


FIGURE 4. (Colour online) Spin-down of containers $f(\tau)$ versus τ following an impulsive acceleration for differently shaped vessels. The solid (black online), dashed (red online) and dot-dashed (blue online) curves correspond to a cylinder, sphere and cone, respectively. The radius of the sphere equals the radius and half-height of the cylinder and the base radius and half-height of the cone. For all shapes, the model parameters are $K = 1$, $B = 1$, $B' = 0$, $E = 0.005$, $\rho_n = 0.25$ and $\Omega_0 = \Omega_{n0} = 0$.

Having studied the container response in different geometries, we now consider flows in which the fluid components are initially differentially rotating. In figure 5, we present a spin-down for a spherical container where the viscous and inviscid components are differentially rotating at $\tau = 0$. The initial conditions are $\Omega_{n0} = 0.3$ and $\Omega_0 = 0.7$, so that the initial angular velocity of the inviscid component is $\Omega_{s0} = (\Omega_0 - \Omega_{n0}\rho_n)/(1 - \rho_n) = 0.83$. The differential rotation may arise in practice when large numbers of vortices unpin collectively, redistributing angular momentum in the inviscid component. This phenomenon is observed in type II superconductivity

https://doi.org/10.1017/jfm.2014.84 Published online by Cambridge University Press

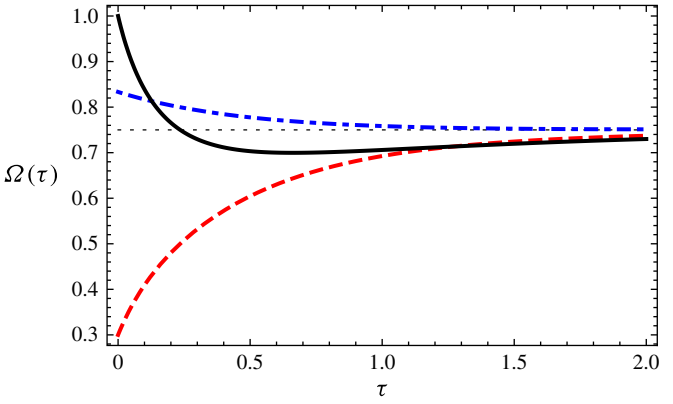


FIGURE 5. (Colour online) Spin-down of a spherical container following an impulsive increase in angular momentum, with initial differential rotation between the inviscid and viscous fluid components. Model parameters are $B = 0.01$, $B' = 0$, $E = 5 \times 10^{-5}$, $\rho_n = 0.25$, $K = 5$, $\Omega_{n0} = 0.3$ and $\Omega_0 = 0.7$ ($\Omega_{s0} = 0.83$). The solid curve (black online) represents the angular velocity of the container, and the dashed (red online) and dot-dashed (blue online) curves represent the angular velocities of the viscous and inviscid fluid components at $r = 0.5$, respectively. The grey dotted line is the steady-state solution (4.3).

and is believed to be responsible for pulsar glitches (Anderson *et al.* 1978). When the fluid components initially rotate differentially, a more diverse range of spin-down curve shapes are observed. An example is presented in figure 5, where the container 'overshoots', i.e. the angular velocity of the container (plotted as a solid black curve) drops below the asymptotic value before rising again. The fluid components are coupled in the intermediate regime ($BE^{-1/2} = 1.41$). The angular velocities of the viscous and inviscid components of the fluid at $r = 0.5$ are plotted as dashed and dot-dashed curves, respectively, to demonstrate the mechanism of the overshoot. The container, which is relatively light ($K = 5$), and the viscous component are drawn together quickly by viscous forces. They then approach the inviscid component together over the mutual friction time scale.

In figure 6, we present a general example of the solution in § 3.1, demonstrating its full utility. The spin-down of a conical container is plotted, where the base of the cone is not rigidly connected to its upper surface. At $\tau = 0$, the upper section and the base are impulsively accelerated to $f_{u0} = 1$ and $f_{l0} = -0.5$, respectively. Their subsequent motions are represented as the upper and lower solid black curves in figure 6, respectively. The viscous and inviscid fluid components (plotted as dashed and dot-dashed curves, respectively) are also initially differentially rotating, with $\Omega_{n0} = 0.6$ and $\Omega_0 = 0.2$ ($\Omega_{s0} = 0.067$). The coupling of the fluid components is in the intermediate regime, with $BE^{-1/2} = 1$. First, the angular velocity of the viscous component becomes the average of the upper section and base. Viscous forces then bring the upper section and the base into co-rotation. Finally, co-rotation with the inviscid component is established over the mutual friction time scale.

In figure 7 the fluid motion inside the cone is plotted at $\tau = 1$. The viscous and inviscid fluid velocities are plotted in panels (*a*) and (*b*), respectively. The shading represents the magnitude of the angular velocities (in the rotating frame), where dark represents zero and light represents unity (spin-up). The azimuthal velocity is computed from (2.74) and (2.75) with boundary layer corrections (2.57)–(2.61)

https://doi.org/10.1017/jfm.2014.84 Published online by Cambridge University Press

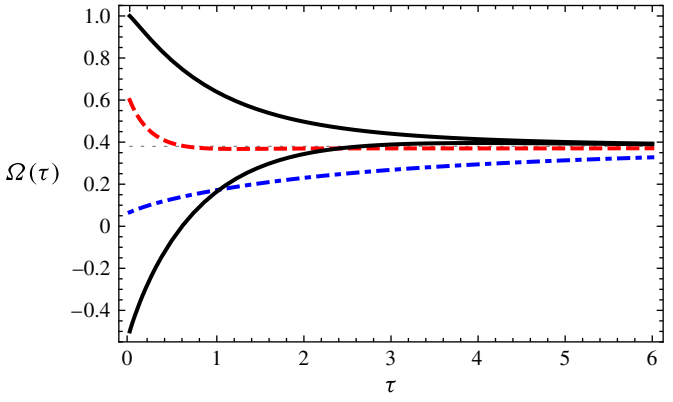


FIGURE 6. (Colour online) Spin-down curve of a cone (whose upper surface in not rigidly connected to its base), following differential spin-up of the cone and base. Model parameters are $B = 0.01$, $B' = 0$, $E = 1 \times 10^{-4}$, $\rho_n = 0.25$, $K_u = 1$, $K_l = 2$, $f_{u0} = 1$, $f_{l0} = -0.5$, $\Omega_{n0} = 0.6$ and $\Omega_0 = 0.2$ ($\Omega_{s0} = 0.07$). The upper and lower solid curves (black online) represent the angular velocity of the upper and lower container lids, respectively. The dashed (red online) and dot-dashed (blue online) curves represent the angular velocities of the viscous and inviscid fluid components at $r = 0.5$, respectively. The grey dotted line is the steady-state solution (4.3).

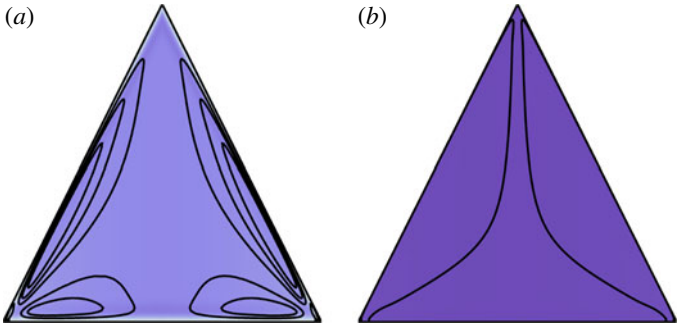


FIGURE 7. (Colour online) Slices of the meridional flow for the (*a*) viscous and (*b*) inviscid components for the spin-down of the cone in figure 6 at $\tau = 1$. Poloidal flow is clockwise on the upper right-hand side, anticlockwise on the lower right-hand side and mirrored about the rotation axis in both panels. (*a*) Contours (from right wall down): -0.15, -0.10, -0.05, 0.05, 0.10. (*b*) Contour -0.0004. The magnitude of the angular velocity (in the frame rotating with the container) is shaded, where dark is zero and light is unity (spun up).

in van Eysden & Melatos (2013). The contours represent the streamfunction for the poloidal flow, and are computed from (2.76) and (2.77) with boundary layer corrections (2.50)–(2.54) in van Eysden & Melatos (2013). Ekman pumping in the inviscid component is weak because the fluids are coupled in the intermediate regime. Figure 7 demonstrates the generality of the solution presented in van Eysden & Melatos (2013); the velocity fields for both fluid components can be plotted for any geometry and any motion of the container.

In all the cases presented in § 4, the container angular velocity approaches a steady-state value as $\tau \to \infty$. The steady-state angular velocity can easily be determined from

https://doi.org/10.1017/jfm.2014.84 Published online by Cambridge University Press

the results derived in van Eysden & Melatos (2013). The time derivatives of (3.2) and (3.3) imply that

$$f_u(\infty) = f_l(\infty) = f_\infty. \tag{4.1}$$

Equations (2.74) and (2.75) in van Eysden & Melatos (2013) imply that

$$v^I_\phi(\infty) = v^I_{n\phi}(\infty) = rf_\infty, \tag{4.2}$$

and hence the system tends towards rigid-body co-rotation. Upon substituting (4.1) and (4.2) into (3.12) and assuming Ω_0 is uniform, in terms of scaled variables we obtain

$$f_\infty = \frac{f_{u0}K_l + f_{l0}K_u + K_lK_u\Omega_0}{K_u + K_l + K_lK_u}. \tag{4.3}$$

This steady-state solution is plotted as a thin horizontal dotted grey line in figures 5 and 6.

The initial angular acceleration of the upper and lower lids of the container can also be calculated analytically. Because the initial spin-down rate of the container is related directly to the superfluid parameters, these results are particularly useful for measuring B, B', ρ_n and E when they are unknown. Applications include potential laboratory experiments (van Eysden & Melatos 2012, 2011), and measuring the properties of bulk nuclear matter in neutron stars (van Eysden & Melatos 2010).

Evaluating the time derivative of (3.5) and (3.6) at $\tau = 0$ we obtain

$$\dot{f}_u(0) = -K_u(f_{u0} - \Omega_{n0})[\dot{g}^A_{uu}(0) + \dot{g}^A_{ul}(0)] + \frac{K_uT^{ext}_u(0)}{I_fE^{1/2}}, \tag{4.4}$$

$$\dot{f}_l(0) = -K_l(f_{l0} - \Omega_{n0})[\dot{g}^A_{ul}(0) + \dot{g}^A_{ll}(0)] + \frac{K_lT^{ext}_l(0)}{I_fE^{1/2}}. \tag{4.5}$$

The functions $\dot{g}^A(0)$ depend on $J_{u,l}$, and hence B, B', ρ_n. In the weak coupling regime, $J_{u,l} = \rho_nH_{u,l}$, and (4.4) and (4.5) are independent of B and B'. In the classical limit $J_{u,l} = H_{u,l}$ and (4.4) and (4.5) depend on the geometry, moment of inertia of the container and the initial conditions $T^{ext}(0), f_{u,l}$ and Ω_{n0}.

5. Response to an external torque

We now investigate the response of the container with some simple external driving torques. Two cases are considered: a constant and an oscillating torque.

5.1. *Constant torque*

The spin-down of containers subject to a constant external torque has many applications, including laboratory experiments that have friction in the apparatus (Tsakadze & Tsakadze 1980), or neutron stars, where the solid crust experiences an electromagnetic braking torque (Lyne & Graham-Smith 1998). In this section we consider containers subject to a constant external torque $T^{ext} = T_0$.

In figure 8 we plot the spin-down of a one-piece spherical container following an impulsive acceleration with $T_0 = -0.023$. The mutual friction coupling is in the intermediate regime, with $BE^{-1/2} = 1$. A value of $K = 1$ is chosen so that the time scale for the container response is comparable to the mutual friction and Ekman time scales. The container and fluid undergo a transient response before settling in a

https://doi.org/10.1017/jfm.2014.84 Published online by Cambridge University Press

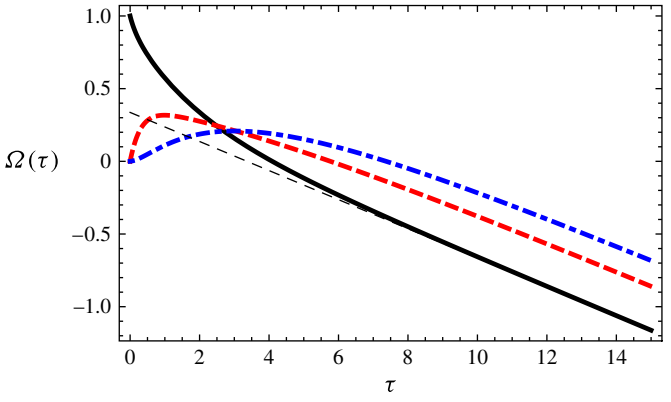


FIGURE 8. (Colour online) Angular velocity versus time for a sphere subject to a constant external torque, following impulsive acceleration. Model parameters are $B = 0.141$, $B' = 0$, $E = 0.005$, $\rho_n = 0.25$, $K = 1$ and $\Omega_{n0} = \Omega_0 = 0$. The solid curve (black online) represents the angular velocity container. The dashed (red online) and dot-dashed (blue online) curves represent the angular velocities of the viscous and inviscid fluid components at $r = 0.5$, respectively. The black dashed curve is the asymptotic result (5.1).

stationary state as $\tau \to \infty$, in which the container and interior fluid components spin down at a constant rate. In the transient phase, both fluid components spin up briefly before beginning to spin down. In the stationary state, the container is lagged by the viscous component of the fluid, which is in turn lagged by the inviscid component. The lag between the viscous component and container depends on the viscosity, while the lag between the viscous and inviscid components depends on the mutual friction, i.e. for strong mutual friction the components are coupled. The fluid components do not undergo rigid-body rotation, but continue to spin down via Ekman pumping.

In figure 9 we plot the flow inside the sphere at $\tau = 1$ (a, b) and in the stationary state, where $\tau = 15$ (c, d). The viscous and inviscid fluid velocities are plotted in panels (a, c) and (b, d), respectively. The angular velocities are shaded, where lighter (darker) means that the angular velocity is higher (lower). In panels (a, b) the angular velocity is plotted with respect to the initial angular velocity of the fluid, while in panels (c, d), it is plotted with respect to the angular velocity of the container (see figure 8). In panels (a, b), both fluid components rotate more slowly than the container. The poloidal flow is clockwise because the fluid is spinning up. In panels (c, d), both fluid components rotate more quickly than the container and the poloidal flow is anticlockwise because the fluid is spinning down.

A useful analytic solution to (3.13) can be obtained in the asymptotic regime, when the container is decelerating linearly. Assuming the angular velocity of the container has the form

$$f_u(\tau) = f_\infty + \alpha\tau, \tag{5.1}$$

as $\tau \to \infty$, the velocity of the fluid components is found using (2.74) and (2.75) in van Eysden & Melatos (2013). We obtain

$$v^I_{n\phi}(\tau) = r\left[f_\infty - \frac{\alpha(h_u + h_l)}{J_u + J_l} + \alpha\tau\right], \tag{5.2}$$

$$v^I_{\phi}(\tau) = r\left\{f_\infty - \alpha\left[\frac{h_u + h_l}{J_u + J_l} + \frac{I_u + I_l}{\beta(J_u + J_l)} - \frac{1}{\beta}\right] + \alpha\tau\right\}. \tag{5.3}$$

https://doi.org/10.1017/jfm.2014.84 Published online by Cambridge University Press

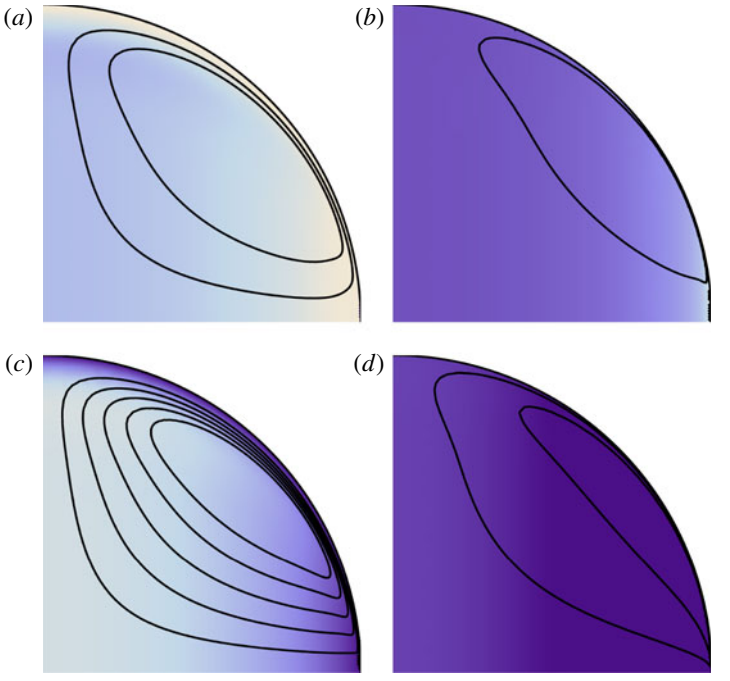


FIGURE 9. (Colour online) Slices of the meridional flow for the viscous (a, c) and inviscid (b, d) components for intermediate coupling $(BE^{-1/2} = 1)$. (a, b) Snapshots at $\tau = 1$ where the poloidal flow is clockwise with streamfunction contours (a) -0.01, -0.025 and (b) -0.0008. (c, d) Snapshots in the asymptotic regime $\tau = 15$ where the poloidal flow is anticlockwise with contours (c) 0.1, 0.2, 0.3, 0.4, 0.5 and (d) 0.0005. The magnitude of the angular velocity is shaded, where lighter (darker) means the angular velocity of the fluid is higher (lower).

Substituting (5.1) into (3.13) gives

$$f_\infty = \frac{1}{1+K}\left\{1 + \Omega_0 K + \frac{2\pi K\alpha}{I_f}\int_0^R \mathrm{d}r\, r^3 (h_u + h_l)\left[\frac{h_u + h_l}{J_u + J_l} + \frac{I_u + I_l}{\beta(J_u + J_l)} - \frac{1}{\beta}\right]\right\}, \quad (5.4)$$

$$\alpha = \frac{KT_0}{I_f E^{1/2}(1+K)}. \quad (5.5)$$

Equations (5.1), (5.4) and (5.5) are a solution to the governing equations (3.13), (2.74) and (2.75) in van Eysden & Melatos (2013). For a decelerating torque, T_0 and α are negative. This result is useful for verifying numerical calculations, e.g. it is plotted as a thin dashed line in figure 8.

5.2. *Oscillating cylinder*

In this section, we consider a rigid cylindrical vessel (whose top and bottom halves are locked together) filled with superfluid and spun up to a constant velocity Ω. This steady state is then perturbed by applying an external oscillating torque of the dimensional form

$$T^{*ext} = \mathrm{i}\epsilon\Omega\omega_d^* I_u^* A \mathrm{e}^{\mathrm{i}\omega_d^* t}. \quad (5.6)$$

https://doi.org/10.1017/jfm.2014.84 Published online by Cambridge University Press

In the absence of a hydrodynamic torque, (5.6) drives the cylinder with angular velocity in the laboratory frame $\Omega + \epsilon\Omega A e^{i\omega_d^* t}$; see (3.1). In dimensionless form (5.6) is

$$T^{ext} = i\omega_d E^{1/2} I_f A e^{i\omega_d \tau}/K. \tag{5.7}$$

In a cylinder, $h_u(r) = h_l(r) = 1$ and hence (2.6)–(2.9), (3.9) and (3.10) are independent of r. We drop the u, l subscripts as the container is symmetric. Equation (3.13) has the following solution:

$$f(\tau) = (f_0 - f_\infty - C - D)\exp(\varpi_+\tau) + C\exp(\varpi_-\tau) + D\exp(i\omega_d\tau) + f_\infty, \tag{5.8}$$

where

$$\varpi_\pm = -\frac{1}{2}\left(\beta + \frac{I+JK}{h}\right) \pm \left\{\left[\frac{1}{2}\left(\beta + \frac{I+JK}{h}\right)\right]^2 - \frac{\beta J(1+K)}{h}\right\}^{1/2}, \tag{5.9}$$

$$C = \frac{\varpi_+ K[\beta(f_0 - \Omega_0) + \varpi_-(f_0 - \Omega_{n0})]}{(1+K)\beta(\varpi_+ - \varpi_-)} + \frac{i\omega_d A\varpi_+ K(\varpi_- + \beta)}{(1+K)\beta(\varpi_+ - \varpi_-)(\varpi_- - i\omega_d)}, \tag{5.10}$$

$$f_\infty = \frac{f_0 + K\Omega_0 - A}{1+K}, \tag{5.11}$$

$$D = \frac{A(\omega_- - i\omega_d)(\omega_+ - i\omega_d)}{(\varpi_- - i\omega_d)(\varpi_+ - i\omega_d)}. \tag{5.12}$$

Equation (5.8) can be verified by substitution into (3.13). The exponents $\varpi_\pm$ reduce to $\omega_\pm$ when $K \to 0$, i.e. for an infinitely heavy container. Equation (5.8) resembles the general motion of a driven, damped, simple harmonic oscillator. The first two terms are the complementary solutions – the free response, which dies away on natural time scales. In (5.11), f_∞ is a result of our choice of rotating reference frame, which does not coincide with the angular velocity of the midpoint of the oscillation. The last term is the driven response and corresponds to the long-term oscillation. The damping in the system is a result of the viscous forces and the dissipative component of the mutual friction force (with coefficient B). At $\tau = 0$ the amplitude of the oscillation is given by f_0, and the angular velocity of the total fluid flux is $r\Omega_0$ in the rotating frame. In contrast to the harmonic oscillator, the initial angular velocity of the container is related to the driving torque. Evaluating the derivative of (3.13) at $\tau = 0$, we obtain

$$\dot{f}(0) = K(\Omega_{n0} - f_0)\dot{g}^A(0) + i\omega_d A. \tag{5.13}$$

In figure 10, we plot the solution (5.8) for $\omega_d = 4\pi$, $K = 10$ and $\rho_n = 0.25$. Panel (a) has $B = B' = 1$, while panel (b) has $B = B' = E^{1/2}$, for $E = 0.0001$, $A = 0.5$ and $f_0 = 1$ in both panels. In each case, we see a transient decay over the characteristic time $\tau = 1$, corresponding to the Ekman time. In panel (a) this decay is more rapid than in panel (b), where the mutual friction is weaker. At large τ the system relaxes to a steady-state oscillation at frequency ω_d, centred at f_∞. The phase and amplitude of the oscillation are dependent on the driving torque and the fluid variables. This relationship can be determined from (5.12). For the amplitude we obtain

$$|D| = A\left[\frac{(\omega_d^2 + \omega_+^2)(\omega_d^2 + \omega_-^2)}{(\omega_d^2 + \varpi_+^2)(\omega_d^2 + \varpi_-^2)}\right]^{1/2}, \tag{5.14}$$

https://doi.org/10.1017/jfm.2014.84 Published online by Cambridge University Press

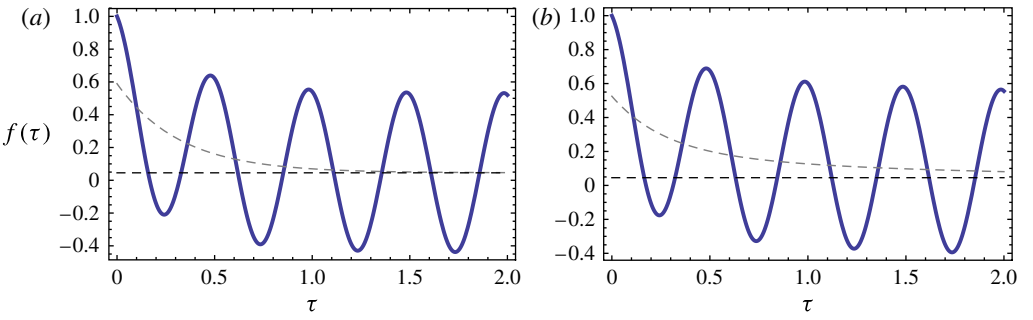


FIGURE 10. Amplitude of oscillation of a rotating cylinder in response to a driving torque at $\omega_d = 4\pi$ with $K = 10$, $\rho_n = 0.25$ and $E = 0.0001$, with (*a*) $B = B' = 1$ and (*b*) $B = B' = E^{1/2}$.

while the phase lag θ is given by

$$\begin{aligned}\tan\theta &= \arg(D)\\ &= \frac{\omega_d\{\omega_d^2(\omega_- + \omega_+ - \varpi_- - \varpi_+) + [\omega_-\omega_+(\varpi_- + \varpi_+) - \varpi_-\varpi_+(\omega_- + \omega_+)]\}}{\omega_d^4 + \omega_d^2[(\varpi_- + \varpi_+)(\omega_- + \omega_+) - \omega_-\omega_+ - \varpi_-\varpi_+] + \varpi_-\varpi_+\omega_-\omega_+}.\end{aligned} \tag{5.15}$$

In figure 11, we plot the phase lag (*a*, *c*) and oscillation amplitude (*b*, *d*) against the driving frequency for three separate cases: strong coupling $B = B' = 1$ (solid), intermediate coupling $B = B' = E^{1/2}$ (dashed) and weak coupling $B = B' = E$ (dot-dashed). Panels (*a*, *b*) have $K = 10$, while panels (*c*, *d*) have $K = 0.1$. The remaining parameters are taken to be $E = 0.0001$ and $\rho_n = 0.25$. Panels (*a*, *c*) indicate that the phase lag vanishes as $\omega_d \to 0$ and $\omega_d \to \infty$, and typically reaches a maximum in the neighbourhood of $\omega_d = 1$, or $\omega_d^* = E^{1/2}\Omega$ in terms of dimensionless variables. For a fluid with an unknown viscosity, the driving frequency may be 'tuned' to this natural 'resonance' to extract the Ekman number, and hence the viscosity.

In figure 11(*b*, *d*), we plot the amplitude of the cylinder motion as a function of driving frequency. The amplitude of the response varies from $A/(1+K)$ when $\omega_d \ll 1$ to A when $\omega_d \gg 1$. The transition between these two states coincides with the maximum in the phase. When there is one peak the amplitude increases in a single step, and when there are two peaks the amplitude increases in two distinct steps. Comparing the upper panels with the lower panels, we note that the phase shift and the change in oscillation amplitude are more pronounced when K is larger (*a*, *b*). The effects shown in figure 11 are most pronounced for $K \sim 10$ and do not significantly increase for higher K.

The phase and amplitude response of the container can be used to constrain the transport coefficients and density fraction of the superfluid. Consistent with the findings in van Eysden & Melatos (2013), the response of the system depends on how strongly the superfluid components are coupled. When $B = B' = 1$ (solid curves), one maximum is observed. Expanding (5.15) in large $\beta = BE^{-1/2}$, this occurs at approximately

$$\omega_d \sim J(1+K)^{1/2}\left[1 + \frac{(J-I)}{\beta}\right] \tag{5.16}$$

https://doi.org/10.1017/jfm.2014.84 Published online by Cambridge University Press

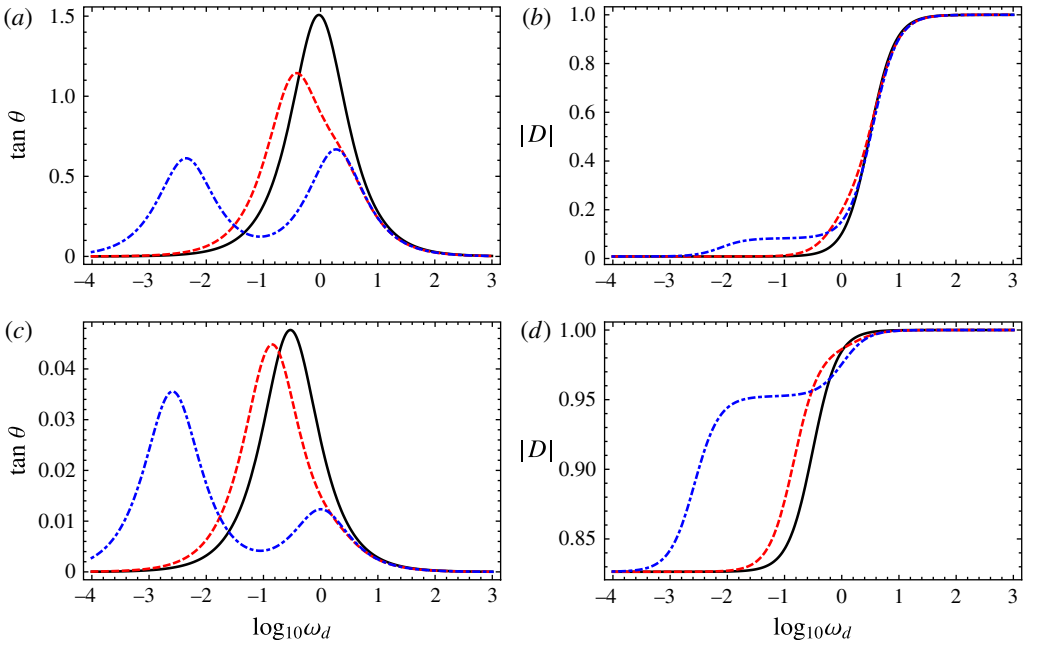


FIGURE 11. (Colour online) (*a*, *c*) Phase and (*b*, *d*) amplitude response of a cylinder with (*a*, *b*) $K = 10$ and (*c*, *d*) $K = 0.1$ subject to an oscillatory driving torque. The curves correspond to strong ($B = B' = 1$; solid, black online), intermediate ($B = B' = E^{1/2}$; dashed, red online) and weak coupling ($B = B' = E$; dot-dashed, blue online). We choose $E = 0.0001$, $\rho_n = 0.25$ and $A = 0.5$.

to order β^{-1}. At this maximum, the phase and amplitude are given by

$$\tan\theta = \frac{K}{2(1+K)^{1/2}}\left[1 - \frac{J^2(J-I)(2+K)^2}{2\beta^3}\right], \tag{5.17}$$

$$|D| = \frac{A}{(1+K)^{1/2}}\left[1 + \frac{J(J-I)K}{\beta^2}\right], \tag{5.18}$$

both of which are weakly dependent on B, B', E and ρ_n. To leading order, changing the fluid parameters only shifts the maximum left or right; there is no change to the size or shape of the peak. Therefore, when the superfluid components are strongly coupled, there is only one measurement with which the fluid parameters can be constrained, namely ω_d. This strong coupling case is the most relevant to helium II above $\sim$1 K, where B and B' are of order unity and there is a non-zero amount of normal component.

As B and B' are decreased, a second maximum is present. Applying Descartes' rule of signs to the derivative of (5.15), it can be shown that there will be two maxima (and one minimum) approximately when

$$BE^{-1/2} < \frac{1}{4}\{[8(1+K\rho_n) + (1-\rho_n)^2]^{1/2} - (1-\rho_n)\}. \tag{5.19}$$

For intermediately and weakly coupled superfluid components, the driving frequencies at which the maxima occur do not have a concise analytical form. Finding the location

https://doi.org/10.1017/jfm.2014.84 Published online by Cambridge University Press

of the maxima and minima in the limit $\beta \ll 1$ is also problematic because two of the three solutions are zero to leading order and possess singularities at order β in their series expansion. The remaining solution, corresponding to the maximum with the largest ω_d, is

$$\omega_d \sim (1+\rho_n K)^{1/2}\left[1-\frac{\beta(1-\rho_n)(2+\rho_n K)^2}{2(1+\rho_n K)^2}\right] \tag{5.20}$$

to order β. The phase and amplitude for this maximum are

$$\tan\theta = \frac{\rho_n K}{2(1+\rho_n K)^{1/2}}\left[1+\frac{\beta(1-\rho_n)(2+\rho_n K)^2}{2(1+\rho_n K)^2}\right], \tag{5.21}$$

$$|D| = \frac{A}{(1+\rho_n K)^{1/2}}\left[1-\frac{\beta\rho_n K(1-\rho_n)(2+\rho_n K)}{2(1+\rho_n K)^2}\right], \tag{5.22}$$

which depends strongly on ρ_n, but is weakly dependent on B, B' and E, as β is small. The results (5.16)–(5.22) can be used in conjunction with amplitude and phase measurements of an oscillating cylinder to constrain B, B', E and ρ_n, in principle.

6. Conclusions

The self-consistent coupled response of a superfluid and its container to an impulsive acceleration has been calculated for the first time. The container responds to the hydrodynamic torque exerted by the superfluid and an arbitrary external torque. The theory describes containers of arbitrary shape, including those in which the top and bottom halves can rotate separately. Angular momentum is conserved overall, unlike in the classical spin-up problem (Greenspan & Howard 1963; Pedlosky 1967; Abney & Epstein 1996), where the rotation of the container is prescribed.

When there is no external torque, and the container is light compared with the total amount of fluid, the spin-down time t_0 is shorter than the Ekman time and weakly depends on E and B. But t_0 depends strongly on E and B when the container is heavy. Containers that are shorter (measured along their rotation axis) have shorter t_0. When the viscous and inviscid fluid components are initially differentially rotating, the spin-down of the container can be non-monotonic, 'overshooting' its asymptotic value.

Two external driving torques are considered: a constant torque and an oscillating torque. Under a constant torque the long-term angular velocity of the container is linear in time, where the viscous component lags the container and the inviscid component lags the viscous component. An exact solution is derived for an oscillating torque, where the oscillation amplitude of the container is largest when driven on the Ekman time scale and when $K \sim 10$. The phase and amplitude response of the cylinder can be used to constrain the transport coefficients and density fraction of the contained superfluid, in principle.

The results derived have many applications, including pulsar astronomy (van Eysden & Melatos 2010) and terrestrial He II experiments (van Eysden & Melatos 2012, 2011), which are discussed in companion papers.

Acknowledgements

C.A.V.E. acknowledges the financial support of an Australian Postgraduate Award. This work was also supported by a Discovery Project grant from the Australian Research Council.

https://doi.org/10.1017/jfm.2014.84 Published online by Cambridge University Press

Appendix A. Approximate and exact analytic solutions

The analytic solution (5.8) has many applications. We present some useful forms here.

A.1. *Weak and intermediate mutual friction*

In many applications, such as pulsars, the superfluidity coefficients satisfy $E^{1/2} \ll B, B' \ll 1$. In this limit, the exact solution in a cylinder (5.8)–(5.12) with no external torque reduces to

$$J = \rho_n H, \tag{A 1}$$

$$I = H, \tag{A 2}$$

$$\varpi_+ = -\frac{\rho_n H(1+K)}{h}, \tag{A 3}$$

$$\varpi_- = -\beta, \tag{A 4}$$

$$C = \frac{H\rho_n K(\Omega_0 - \Omega_{n0})}{\beta h - \rho_n H(1+K)}. \tag{A 5}$$

A.2. *Approximation for a sphere*

When the mutual friction is weak $E^{1/2} \ll B, B' \ll 1$, (5.8) can be used to approximate the spin-down of a sphere. Approximating

$$H = \frac{20h}{7} \tag{A 6}$$

and using the definitions (A 1)–(A 5), (5.8) is a good approximation for $K\rho_n \sim BE^{-1/2}$. This solution matches the exact solution to $\leqslant 1\,\%$ for $BE^{-1/2} \geqslant 10^3$.

A.3. *Classical fluid*

For a one-component Navier–Stokes fluid, one has $B = B' = 0$, $\rho_n = 1$ and $\Omega_{n0} = \Omega_0$. Therefore $I = J = H$, $\omega_- = \beta = 0$ and $\omega_+ = -H/h$. Equation (3.13) reduces to

$$f(\tau) = -K\int_0^\tau \mathrm{d}\tau'\, \dot{g}^A(\tau - \tau')f(\tau') + Kg^A(\tau)\Omega_0 + 1 + \int_0^\tau \mathrm{d}\tau' T^{ext}(\tau'), \tag{A 7}$$

with

$$g^A(\tau) = -\frac{4\pi}{I_f}\int_0^R \mathrm{d}r\, r^3 h(\mathrm{e}^{-H\tau/h} - 1), \tag{A 8}$$

$$g^B(\tau) = 0. \tag{A 9}$$

For the solution in a cylinder, (5.9)–(5.12) reduce to $\varpi_- = 0 = B$ and $\varpi_+ = -H(1+K)/h$.

REFERENCES

ABNEY, M. & EPSTEIN, R. I. 1996 Ekman pumping in compact astrophysical bodies. *J. Fluid Mech.* **312**, 327–340.

ABNEY, M., EPSTEIN, R. I. & OLINTO, A. V. 1996 Observational constraints on the internal structure and dynamics of the Vela pulsar. *Astrophys. J. Lett.* **466**, L91.

https://doi.org/10.1017/jfm.2014.84 Published online by Cambridge University Press

AMBERG, G. & UNGARISH, M. 1993 Spin-up from rest of a mixture: numerical simulation and asymptotic theory. *J. Fluid Mech.* **246**, 443–464.

ANDERSON, P. W. & ITOH, N. 1975 Pulsar glitches and restlessness as a hard superfluidity phenomenon. *Nature* **256**, 25–27.

ANDERSON, P. W., PINES, D., RUDERMAN, M. & SHAHAM, J. 1978 Questions about rotating superfluid dynamics: problems of pulsar astrophysics accessible in the laboratory. *J. Low Temp. Phys.* **30**, 839–847.

BENNETT, M. F., VAN EYSDEN, C. A. & MELATOS, A. 2010 Continuous-wave gravitational radiation from pulsar glitch recovery. *Mon. Not. R. Astron. Soc.* **409**, 1705–1718.

BENTON, E. R. & CLARK, A. 1974 Spin-up. *Annu. Rev. Fluid Mech.* **6**, 257–280.

BENTON, E. R. & LOPER, D. E. 1969 On the spin-up of an electrically conducting fluid. Part 1. The unsteady hydromagnetic Ekman–Hartmann boundary-layer problem. *J. Fluid Mech.* **39**, 561–586.

CLARK, A., CLARK, P. A., THOMAS, J. H. & LEE, N.-H. 1971 Spin-up of a strongly stratified fluid in a sphere. *J. Fluid Mech.* **45**, 131–149.

DONNELLY, R. J. 2005 *Quantized Vortices in Helium II*. Cambridge University Press.

DUCK, P. & FOSTER, M. 2001 Spin-up of homogeneous and stratified fluids. *Annu. Rev. Fluid Mech.* **33**, 231–263.

EASSON, I. 1979 Postglitch behavior of the plasma inside neutron stars. *Astrophys. J.* **228**, 257–267.

ESPINOZA, C. M., LYNE, A. G., STAPPERS, B. W. & KRAMER, M. 2011 A study of 315 glitches in the rotation of 102 pulsars. *MNRAS* **414**, 1679–1704.

VAN EYSDEN, C. A. & MELATOS, A. 2008 Gravitational radiation from pulsar glitches. *Class. Quantum Grav.* **25** (22), 225020.

VAN EYSDEN, C. A. & MELATOS, A. 2010 Pulsar glitch recovery and the superfluidity coefficients of bulk nuclear matter. *Mon. Not. R. Astron. Soc.* **409**, 1253–1268.

VAN EYSDEN, C. A. & MELATOS, A. 2011 Spin down of superfluid-filled vessels: theory versus experiment. *J. Low Temp. Phys.* **165**, 1–14.

VAN EYSDEN, C. A. & MELATOS, A. 2012 Interpreting superfluid spin up through the response of the container. *J. Low Temp. Phys.* **166**, 151–170.

VAN EYSDEN, C. A. & MELATOS, A. 2013 Spin-up of a two-component superfluid: analytic theory in arbitrary geometry. *J. Fluid Mech.* **729**, 180–213.

GLABERSON, W. I., JOHNSON, W. W. & OSTERMEIER, R. M. 1974 Instability of a vortex array in He II. *Phys. Rev. Lett.* **33**, 1197–1200.

GLAMPEDAKIS, K. & ANDERSSON, N. 2006 Ekman layer damping of r modes revisited. *Mon. Not. R. Astron. Soc.* **371**, 1311–1321.

GOLDBAUM, D. S. & MUELLER, E. J. 2009 Commensurability and hysteretic evolution of vortex configurations in rotating optical lattices. *Phys. Rev.* A **79** (6), 063625.

GREENSPAN, H. P. 1968 In *The Theory of Rotating Fluids* Cambridge Monographs on Mechanics and Applied Mathematics, Cambridge University Press.

GREENSPAN, H. P. & HOWARD, L. N. 1963 On a time-dependent motion of a rotating fluid. *J. Fluid Mech.* **17**, 385–404.

HEWITT, R. E., DAVIES, P. A., DUCK, P. W. & FOSTER, M. R. 1999 Spin-up of stratified rotating flows at large Schmidt number: experiment and theory. *J. Fluid Mech.* **389**, 169–207.

JACKSON, B. & BARENGHI, C. F. 2006 Hysteresis effects in rotating Bose–Einstein condensates. *Phys. Rev.* A **74** (4), 043618.

JONES, C. A., KHAN, K. B., BARENGHI, C. F. & HENDERSON, K. L. 1995 Appearance of vortices in rotating He II. *Phys. Rev.* B **51**, 16,174–16,184.

LOPER, D. E. 1971 Hydromagnetic spin-up of a fluid confined by two flat electrically conducting boundaries. *J. Fluid Mech.* **50**, 609–623.

LYNE, A. G. & GRAHAM-SMITH, F. 1998 *Pulsar Astronomy*. Cambridge University Press.

LYNE, A. G., SHEMAR, S. L. & SMITH, F. G. 2000 Statistical studies of pulsar glitches. *Mon. Not. R. Astron. Soc.* **315**, 534–542.

MELATOS, A., PERALTA, C. & WYITHE, J. S. B. 2008 Avalanche dynamics of radio pulsar glitches. *Astrophys. J.* **672**, 1103–1118.

https://doi.org/10.1017/jfm.2014.84 Published online by Cambridge University Press

MENDELL, G. 1998 Magnetohydrodynamics in superconducting–superfluid neutron stars. *Mon. Not. R. Astron. Soc.* **296**, 903–912.

PARKER, N. G. & ADAMS, C. S. 2006 Response of an atomic Bose–Einstein condensate to a rotating elliptical trap. *J. Phys. B: At., Mol. Opt. Phys.* **39**, 43–55.

PEDLOSKY, J. 1967 The spin up of a stratified fluid. *J. Fluid Mech.* **28**, 463–479.

PERALTA, C., MELATOS, A., GIACOBELLO, M. & OOI, A. 2005 Global three-dimensional flow of a neutron superfluid in a spherical shell in a neutron star. *Astrophys. J.* **635**, 1224–1232.

REISENEGGER, A. 1993 The spin-up problem in helium II. *J. Low Temp. Phys.* **92**, 77–106.

REISENEGGER, A. & GOLDREICH, P. 1992 A new class of g-modes in neutron stars. *Astrophys. J.* **395**, 240–249.

STEWARTSON, K. 1953 On the flow between two rotating coaxial disks. *Proc. Camb. Phil. Soc.* **49**, 333–341.

TSAKADZE, J. S. & TSAKADZE, S. J. 1972 Relaxation phenomena at accelaration of rotation of a spherical vessel with helium II and relaxation in pulsars. *Phys. Lett.* A **41**, 197–199.

TSAKADZE, J. S. & TSAKADZE, S. J. 1973 Measurement of the relaxation time on acceleration of vessels with helium II and superfluidity in pulsars. *Sov. Phys. JETP* **37**, 918–921.

TSAKADZE, J. S. & TSAKADZE, S. J. 1974 On the problem of relaxation time determination in superfluids when their rotation is accelerated. *Phys. Lett.* A **47**, 477–478.

TSAKADZE, J. S. & TSAKADZE, S. J. 1980 Properties of slowly rotating helium II and the superfluidity of pulsars. *J. Low Temp. Phys.* **39**, 649–688.

VINEN, W. F. & NIEMELA, J. J. 2002 Quantum turbulence. *J. Low Temp. Phys.* **128**, 167–231.

WALIN, G. 1969 Some aspects of time-dependent motion of a stratified rotating fluid. *J. Fluid Mech.* **36**, 289–307.

WANG, N., MANCHESTER, R. N., PACE, R. T., BAILES, M., KASPI, V. M., STAPPERS, B. W. & LYNE, A. G. 2000 Glitches in southern pulsars. *Mon. Not. R. Astron. Soc.* **317**, 843–860.

WARSZAWSKI, L. & MELATOS, A. 2011 Gross–Pitaevskii model of pulsar glitches. *Mon. Not. R. Astron. Soc.* **415**, 1611–1630.

WARSZAWSKI, L., MELATOS, A. & BERLOFF, N. G. 2012 Unpinning triggers for superfluid vortex avalanches. *Phys. Rev.* B **85** (10), 104503.

https://doi.org/10.1017/jfm.2014.84 Published online by Cambridge University Press